2002

Heat and Mass Transfer Coefficients Under Frost Conditions In A Finned-Tube Evaporator

Y. Kim
Korea University

Y. Jang
Korea University

Y. Kim
Korea University

H. Y. Kim
Korea University

R5-4

Heat and Mass Transfer Coefficients under Frost Conditions in a Finned-Tube Evaporator

Yonghan Kim and Yonghee Jang, Graduate Student, Korea University.
Seoul, 136-701, KOREA; E-mail: yonghkim@korea.ac.kr

*Yongchan Kim, PhD, Associate Professor, Dept. of Mechanical Engineering, Korea University.
Seoul, 136-701, KOREA; Tel.: 82-2-3290-3366; Fax: 82-2-921-5439
E-mail: yongckim@korea.ac.kr *Author for Correspondence

Ho Young Kim, PhD, Professor, Dept. of Mechanical Engineering, Korea University.
Seoul, 136-701, KOREA; Tel.: 82-2-3290-3356; E-mail: kimhy@korea.ac.kr

ABSTRACT

The objectives of this study are to provide experimental data and a correlation that can be used in the optimal design of an evaporator under frost conditions. In the present study, we tested both a single stage and a two-stage evaporator with a variation of operating parameters and fin geometry under frost conditions. The effects of tube space and fin alignment on the heat transfer performance were also investigated. The airside heat and mass transfer coefficients were calculated from the measured data. Besides, two correlations for frost thickness and airflow ratio were developed as a function of dimensionless operating parameters and fin geometry.

NOMENCLATURE

A	:	area [m^2]	m	:	frost accumulation [g]
AR	:	airflow ratio	Nu	:	Nusselt number
BR	:	blockage ratio	Q	:	airflow rate [CMM]
D_h	:	hydraulic diameter, $4A_{min}\,L/A_t$ [m]	$\dot{Q}$	:	cooling capacity [W]
F	:	fin pitch [mm]	Re	:	Reynolds number
F_o	:	Fourier number	RH	:	relative humidity
F^*	:	dimensionless fin pitch, F/F_{base} (F_{base}=10)	T	:	temperature [°C]
h	:	heat transfer coefficient	T^*	:	dimensionless temperature, $T_s/(T_s-T_a)$
h_m	:	mass transfer coefficient	ΔT	:	temperature difference between inlet air and frost surface
L	:	fin depth [m]			

W : humidity ratio

ΔW : humidity ratio difference between inlet air and saturated air temperature on the frost surface

Greek letters

δ : thickness [m]

η : fin efficiency

Subscripts

a : air

f : frost

fin : fin

in : inlet

min : minimum

t : total

INTRODUCTION

When moist air passes over a heat exchanger surface, whose temperature is below the freezing point, water vapor condenses and then frost forms in the evaporator surface. Due to the heat and mass transfer of moist air, moisture molecules migrate to the frosted surface and the void portion of the frost layer, which leads to frost growth and densification of the frost layer. Frost accumulation shows both positive and negative effects on the heat transfer. During the early stage of frost formation, the frosted surface improves a local heat transfer coefficient due to relatively higher roughness and an increase of fin efficiency. However, as the frost thickness increases over a limit, the frost layer acts as an insulation layer between the fins and the air. In addition, the frost blocks the airflow path, causing an increase in pressure drop and decrease in airflow rate. Uneven frost formation causes a higher-pressure drop and a larger reduction in airflow rate than those for even frost distribution. Therefore, in order to achieve better heat transfer performance in an evaporator used in a refrigerator, the frost growth process needs to be delayed and the frost has to be formed uniformly over the evaporator surface. If possible, no frost formation will be the best solution.

Most of researches on the frost formation have been focused on simple geometries such as flat plate and round tubes. Several researchers investigated the frost growth and mass accumulation (Hayashi et al. [1], Schropp [2], Kamai et al. [3], Yamakawa et al. [4]). They represented heat transfer characteristics under frost conditions as a function of air temperature, air velocity, and humidity ratio. Recently, Rite and Crawford [5] studied the effects of the frost on the UA value and airside pressure drop in a domestic refrigerator evaporator coil. It was observed that the UA value increased as the frost initially formed on the evaporator, but then the UA significantly decreased as more frost formed on the evaporator. Senshu et al.[6], Oskarsson et al. [7], and Kondepudi and O'Neal [8] tested several evaporator coils under frost conditions. However, these mainly included the frost formation in a heat pump heat exchanger with a higher fin density.

Due to complex geometry of finned-tube heat exchangers and diversity of operating variables, a

further study is required to establish better design tool for uniform frost distribution and delay of frost formation as well. The major objectives of this study are to explore heat and mass transfer characteristics of a refrigerator evaporator and to provide a generalized correlation to predict frost thickness and airflow ratio under frosting conditions.

EXPERIMENTAL SETUP AND TEST PROCEDURE

A schematic of the experimental setup for measurement of heat and mass transfer under frost conditions is shown in Fig. 1. The test setup was installed in a psychrometric chamber to provide low ambient temperature and pre-control capability as well. The psychrometric chamber was maintained at 2°C using an air-handling unit including a cooling coil, a heating coil, and a humidifier. For measurement convenience, the ethylene glycol-water mixture was utilized as a refrigerant inside the coil.

Five operating parameters in the test setup was controlled during the tests: temperature of ethylene glycol-water mixture, airflow rate, inlet air temperature and inlet dew point. Using a constant temperature bath including a chiller and an electric heater controlled the ethylene glycol-water mixture temperature. A close wind tunnel was placed inside of the environmental chamber. Air temperatures were measured by arithmetically averaging T-type thermocouple grid located before and after the test coil. The air temperature entering the test section was adjusted by using both a cooling coil and an electric resistance heater installed at the entrance of the flow chamber. The absolute humidity was measured using a chilled mirror dew point sensor. The humidity was maintained at a set point by adjusting power input to an ultrasonic humidifier using a PID controller.

The frost thickness was measured using a cathetometer and a digital depth meter with an uncertainty of 0.04 mm for smooth frost and approximately an order of magnitude larger for rough frost. The frost surface temperature was measured by using an infrared thermometer with an uncertainty of ± 0.2°C. The fin and tube surface temperatures were measured by using T-type thermocouples. The data was stored in a data logger at every three seconds. The refrigeration capacity of the test coil was determined by an air enthalpy method as well as a waterside capacity, which yielded a good agreement within 5% at the early stage of frost formation.

The test coil is a finned tube heat exchanger with 1-path structure of 2-rows and 1-stage, and has the dimension of 400 mm × 60 mm × 27 mm. We tested three different heat exchangers, which have the identical geometric shape except for fin pitch. The test coils include 39, 32 and 26 fins with a fin pitch of 10.0 mm, 12.5 mm, and 15.0 mm. After investigating the heat and mass transfer performance of each heat exchanger, two heat exchangers are combined to make two-stage coil. Test conditions are specified in Table 1.

RESULTS AND DISCUSSION

Heat Transfer Performance for the Non-Frosting Conditions

Steady state and nearly dry surface tests were conducted to determine the airside heat transfer coefficients for the non-frosting conditions. The airflow rate was varied at 1.0, 1.2, 1.4 and 1.6 CMM, while the air temperature was altered at 1, 3, and 5°C. The dew point was maintained below -15°C. Fig. 2 shows the effects of fin pitch and air temperature on the Nu against the Re. As expected, the Nu increases with an increase of Re for all test samples. As the fin pitch is reduced, the Nu decreases, but the heat transfer rate increases due to a rise of total surface area. In general, the Nu is independent of the temperature difference. In this study, the Nu was independent of the temperature difference at a smaller fin pitch and a higher velocity. However, the Nu increases with a rise of the temperature difference at a larger fin pitch.

Heat Transfer Performance for the Frosting Conditions

The frost thickness and frost accumulation were measured with a variation of inlet air temperature, dew point, airflow rate, fin pitch and refrigerant temperature. According to the experimental results, it is obvious that the frost growth rate increases at a relatively higher humidity, a higher airflow rate, and a lower inlet air temperature. The frost becomes relatively thick at a larger fin pitch. In this case, the frost grows fast at the early stage and then the growth rate gradually decreases due to a densification of the frost layer and a reduction of the airflow rate.

As the frost grows, the effective airflow area decreases and the thermal resistance increases. These trends yield a drop of cooling capacity and efficiency. A correlation for the frost thickness as a function of operating conditions and fin geometry is very useful to determine heat exchanger performance under frost conditions. In this study, the frost thickness was measured at the several points of the fin and then averaged. The correlation for the frost thickness was derived as a function of the dimensionless operating parameters.

$$\delta_f = 2.1436 \times \mathrm{Re}^{0.2367} \times F_o^{\,0.3588} \times T^{*\,0.5390} \times F^{*\,0.3305} \times W^{0.6730} \qquad (1)$$

In Eq. (1), F^* is a dimensionless fin pitch, W is an inlet air humidity ratio, F_o is the Fourier number and T^* is a dimensionless temperature.

The correlation shows that the frost thickness increases proportional to air velocity, air humidity, time and temperature difference between the air and the heat exchanger surface. Fig. 3 shows the comparison of the experimental data with the predicted results using the present correlation. The mean deviation of the predicted frost thickness from the measured was 7%.

Fig. 4 shows the relation between blockage ratio (BR) and airflow ratio (AR). The blockage ratio is defined as the ratio of frost thickness to fin pitch, and the airflow ratio is defined as the ratio of airflow

rate at a given time to the initial airflow rate. Fig. 4 includes all test data having different airflow rate, relative humidity and inlet air temperature. The airflow rate decreases with an increase of blockage ratio at all cases. The drop of airflow rate at a fin pitch of 10.0 mm is relatively significant as compared to the other cases. However, for the fin pitch of 15.0 mm, although the blockage ratio is 0.8, the airflow ratio is kept at 0.8. This would indicate that a larger fin pitch could prevent a severe drop of airflow rate under frost conditions. When the airflow ratio is 0.8, the blockage ratios are 0.52, 0.62, and 0.78 at fin pitches of 10.0, 12.5, and 15.0 mm, respectively.

Fig. 5 shows the relationship between the airflow ratio and the *F/BR* at various fin pitches. For the airflow ratios of 0.8 and 0.9, the ratios of fin pitch to blockage ratio are approximately 20.1 and 27.5, respectively, at all fin pitches. This means that the airflow ratio is a strong function of *F/BR*. Therefore, a generalized correlation for the airflow ratio is developed as a function of *F/BR*.

$$AR = 0.98634 - 1.51374 \times \exp(-0.10403 \times (F/BR)) \quad (2)$$

In this study, the mean deviation of the airflow ratio was 4 %.

Figs. 6 and 7 shows the variations of the heat and mass transfer coefficients at a fin pitch of 12.5 mm and an airflow rate of 1.4 CMM. The heat and mass transfer coefficients were determined by Eqs. (3) and (4), respectively.

$$h = \frac{\dot{Q}}{(\eta \times A_f)\Delta T} \quad (3)$$

$$h_m = \frac{m}{(\eta \times A_f)\Delta W} \quad (4)$$

Generally, the heat and mass transfer coefficients increase with an increase of relative humidity. At the early stage of the frost formation, since the ice crystal forms in a needle-like shape, the rough surface increases the heat and mass transfer coefficients. However, as the frost grows, the ice crystal transforms into a plate-like shape, which causes a decrease of heat and mass transfer coefficients due to a reduction of frost roughness. After 25 minutes, the heat transfer gradually increases due to a rise of air velocity. The mass transfer also gradually increases after 60 minutes.

Fig. 8 shows the variation of cooling capacity for the frost and non-frost (dry) conditions. The cooling capacity for the frost condition increases by 10 % as compared to the non-frosting condition. However, due to the reduction of airflow rate, the cooling capacity for the frost condition becomes less than that of the dry condition after one hour. Fig. 9 shows the effects of tube space and fin alignment on the heat transfer performance when the two-stage heat exchanger was tested. The cooling capacity increases with a decrease of tube space in the staggered tube alignment. However, decreasing tube space yields a bad effect to airflow path. Therefore, the cooling capacity drops significantly after several tens of minutes in the case of narrow tube space and staggered alignment. In the case of in-line alignment, the tube space shows a little effect on cooling capacity. Besides, the tube alignment shows negligible effects

on cooling capacity at large tube spaces.

CONCLUSIONS

The performance of the finned-tube evaporator under frost conditions was experimentally investigated with a variation of operating conditions and heat exchanger geometry. Based on the test results, the correlation for the frost thickness was derived as a function of dimensionless operating parameters. Besides, the airflow ratio was correlated with *F/BR*. The mean deviations of the correlations for the frost thickness and the air flow ratio were 7% and 4%, respectively. For a narrow tube space, the staggered tube alignment improves cooling capacity by 14% as compared to the in-line alignment. However, for a larger tube space the effects of the tube alignment on cooling capacity become negligible.

ACKNOWLEGEMENTS

The authors would like to express sincere thanks to Samsung Electronics Co. Ltd. for the financial support on this project.

REFERENECES

1. Hayashi, Y., Aoki, A., Adachi, S., and Hori, K., “Study of Frost Properties Correlating with Frost Formation Types,” Journal of Heat Transfer, Vol. 99, pp. 239-245, 1977.
2. Schropp, K., “Investigations of Dew and Frost Formation on Cooling Rubes in Still Air and the Influence Upon Heat Transfer,” Zeitschr. Ges. Kalte. Ind., Vol. 42, pp. 81-85, 127-131, 1935.
3. Kami, S., Mizushina, S., Kifune, S., and Koto, T., “Research on the Frost Formation in a Low Temperature Cooler Condenser,” The Japan Science Review, Vol. 2, No. 3, pp. 317-326, 1952.
4. Yamakawa, N., Takahashi, N., and Ohtani, S., “Forced Convection Heat and Mass Transfer under Frost Conditions,” Heat Transfer –Japanese Research, Vol. 1, No. 2, pp. 1-9, 1972.
5. Rite, R.W., and Crawford, R.R., “A Parametric Study of the Factors Governing the Rate of Frost Accumulation on Domestic Refrigerator-Freezer Finned-Tube Evaporator Coils,” ASHRAE Transactions, Vol. 97, pp. 438-446, 1991.
6. Senshu, T., H. Yasuday, K. Oguni, and K. Ishibane., “Heat Pump Performance under Frosting Conditions,” ASHRAE Transactions 96(1), 324-329, 1990.
7. Oskasson, S.P., K.I. Krakow, and S. Lin., “Evaporator Models for Operation with Dry, Wet, and Frosted Finned Surfaces,” ASHRAE Transactions 96(1), 373-379, 1990.
8. Kondepudi, S.N., and D.L. O’Neal, “Frosting Performance of Tube Fin Heat Exchangers with Wavy and Corrugated Fins,” Experimental Thermal and Fluid Science 4, 613-618, 1991.

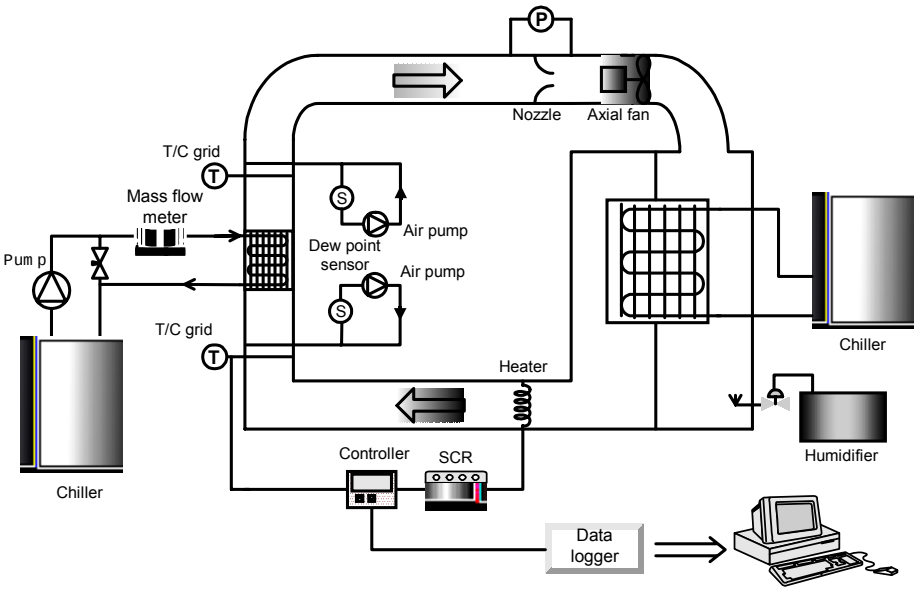

Figure 1: Schematic of the experimental setup.

Table. 1 Test conditions

Parameter	Value		
Inlet air temperature (°C)	1,		3
Inlet air humidity ratio (%)	75,	85,	95
Airflow rate (CMM)	1.2,	1.4,	1.6
Refrigerant inlet temperature (°C)	-20,	-25,	-30

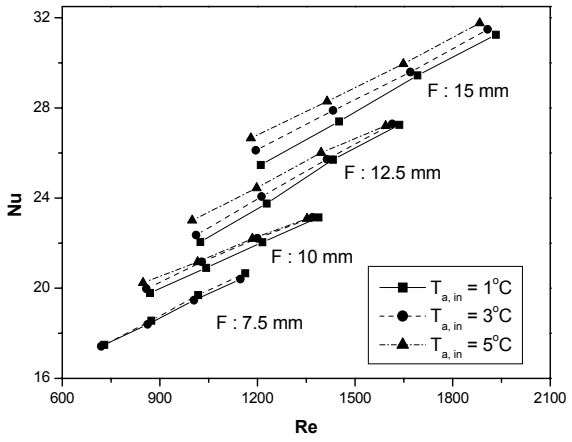

Figure 2: Effects of fin pitch on the NU.

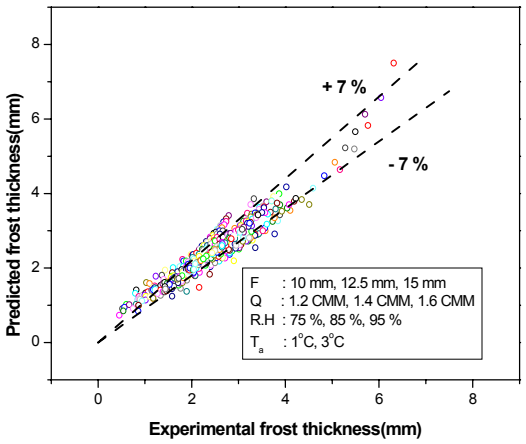

Figure 3: Comparison of frost thickness.

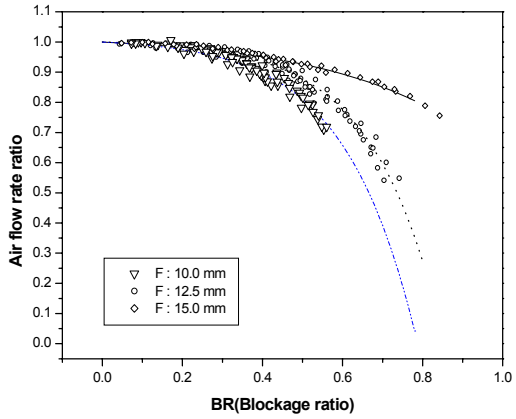

Figure 4: Variation of airflow ratio vs. BR.

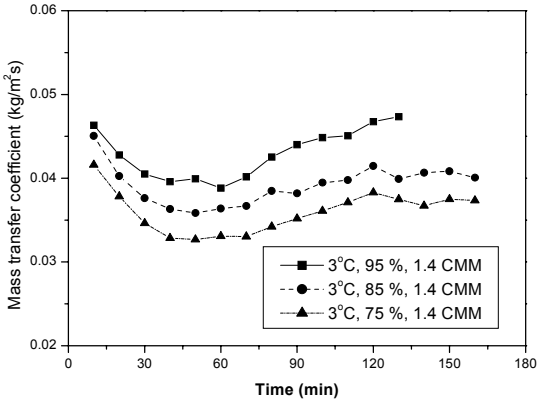

Figure 7: Variation of mass transfer coefficient.

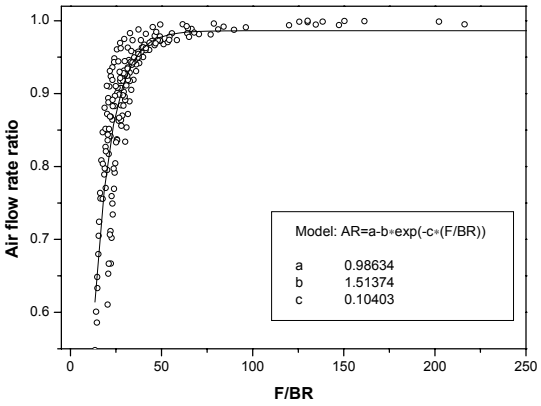

Figure 5: Variation of airflow ratio vs. F/BR.

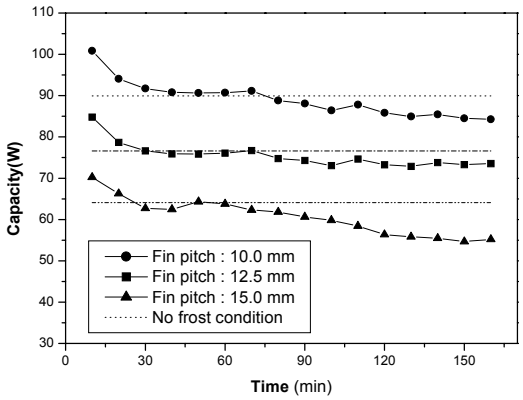

Figure 8: Variation of capacity with fin pitch.

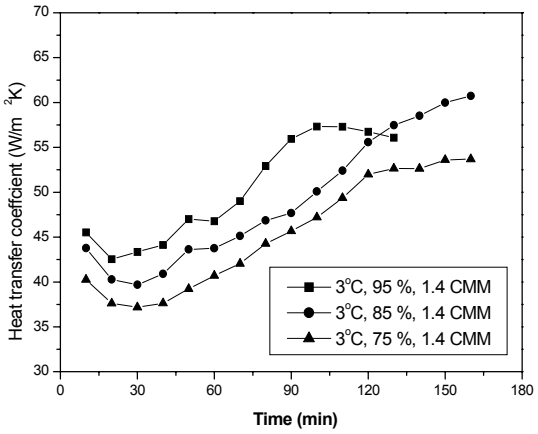

Figure 6: Variation of heat transfer coefficient.

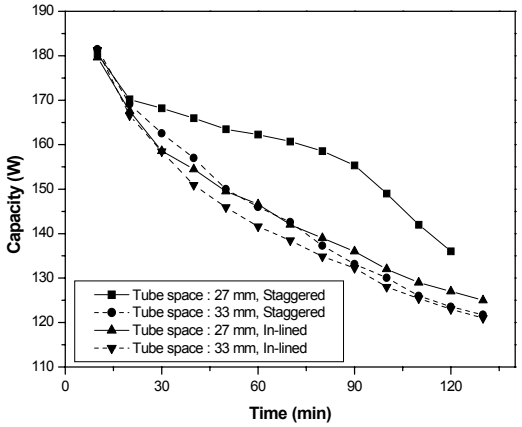

Figure 9: Variation of capacity with tube alignment.